J. Fluid Mech. (2006), *vol.* 555, *pp.* 299–320.
doi:10.1017/S0022112006009104 Printed in the United Kingdom

Variational methods for glacier flow over plastic till

By CHRISTIAN SCHOOF

Department of Earth and Ocean Sciences, University of British Columbia, 6339 Stores Road, Vancouver, BC, V6T 1Z4, Canada
cschoof@eos.ubc.ca

(Received 2 November 2004 and in revised form 24 October 2005)

We investigate the mechanics of ice streams and glaciers flowing over a bed consisting of Coulomb-plastic subglacial sediment, or more generally, of channel flows with Coulomb or 'solid' friction laws at the boundary. Sliding is assumed to occur if shear stress at the glacier bed attains a prescribed, locally defined yield stress, while no sliding is assumed possible below that yield stress. Importantly, the location of regions of slip and no slip at the bed is not known *a priori*, but forms part of the solution. By analogy with friction problems in elasticity, we derive a weak formulation as a semi-coercive variational inequality, which admits a unique solution provided a solvability condition ensuring force balance is satisfied. The variational formulation is then exploited to calculate numerical solutions, and we investigate the effect of variations in subglacial water pressure, ice thickness and surface slope on the discharge of a valley glacier with a plastic bed. Significant differences are found between the behaviour of wide and narrow as well as steep and shallow-angled glaciers, and our results further indicate the need to develop models capable of accounting for longitudinal stresses.

1. Introduction

Many dynamical phenomena in glaciology occur because valley glaciers and ice sheets are able to slide over their beds. For instance, some temperate valley glaciers 'surge', that is, they undergo periodic episodes of dramatic increase in their flow velocities which are associated with rapid lengthening and thinning of the glacier. These surges are thought to be caused by changes in the subglacial meltwater drainage system, which in turn affect the amount of lubrication available at the glacier sole and hence the sliding motion of the glacier (Kamb *et al.* 1985). Similarly, some ice sheets are characterized by the presence of relatively narrow bands of rapidly flowing ice known as ice streams, which are surrounded by more slowly moving ice ridges (Alley & Bindschadler 2001). The high discharge of these ice streams often cannot be explained by shearing in the ice itself, but must be accounted for by rapid sliding at the bed.

The processes by which glaciers and ice sheets are able to slide depend on the physical properties of the underlying bed. If the latter consists of clean, undeformable bedrock, sliding occurs by a combination of regelation and creep deformation around bed undulations (see e.g. Fowler 1981). More commonly, glaciers are underlain by glacial sediments known as till. Sliding in that case occurs as a result of mechanical failure at the ice–till interface or within the till, which is thought to be empirically well-described in both cases by a simple Coulomb failure criterion (Iverson *et al.* 1998, 1999; Tulaczyk 1999; Tulaczyk, Kamb & Engelhardt 2000). If the subglacial till layer is thin compared with the thickness of the overlying ice, the simplest conceivable

boundary condition for ice flow over a deformable bed then takes the form of a 'solid' or Coulomb friction law. This allows for sliding when shear stress at the bed reaches a critical stress τ_c, which in turn is an affine function of compressive normal stress at the bed, while no slip occurs when τ_c is not attained. Under a real glacier, the second of these assumptions may not be realized in practice: even if the bed does not deform, sliding may still occur as a result of processes such as regelation which allow glacier sliding over undeformable beds (similar behaviour arises for sliding over hard beds in the presence of cavitation, see Schoof 2005). In this study, our main interest is the effect of solid friction-type basal boundary conditions on glacier flow rather than a detailed study of physical processes in subglacial till and at the ice–till interface. In this spirit, we assume that sliding velocities are insignificant when the critical shear stress τ_c is not attained, and further ignore a number of other complications which may arise in the deformation of plastic tills (see e.g. dell'Isola & Hutter 1998; Fowler 2003).

Coulomb friction laws as boundary conditions for glacier flow were previously studied by Reynaud (1973) and Pélissier & Reynaud (1974), and interest in the mechanics of glaciers with solid friction at the bed has been revived as a result of experimental studies of till rheology (Truffer, Echelmeyer & Harrison 2001, Schoof 2004*b*). Elsewhere in fluid dynamics, Coulomb friction laws have been used as boundary conditions on viscoplastic materials (e.g. Adams *et al.* 1997; Sherwood & Durban 1998). Both of the earlier papers by Reynaud (1973) and Pélissier & Reynaud (1974) made the assumption that sliding occurs everywhere at the bed. This restricts their channel flow model to the marginal case in which the gravitational driving force on a given glacier cross-section is balanced exactly by the maximum friction force which the bed can exert. By contrast, Truffer *et al.* (2001) and Schoof (2004*b*) were concerned with the case in which sliding does not occur everywhere at the bed, but in which there are patches where the ice is 'stuck' to the bed. This scenario is not only relevant to the flow of valley glaciers when the gravitational driving force is less than the maximum friction force which the bed is able to generate, but is also of central interest in the study of ice streams, where the transition from rapid sliding to no (or little) sliding manifests itself in the form of heavily crevassed 'shear margins' (Harrison, Echelmeyer & Larson 1998; Raymond *et al.* 2001).

Our aim in the present paper is to set out a consistent theoretical framework for studying the glacier flow problem considered in Truffer *et al.* (2001) and Schoof (2004*b*), or more generally, the mechanical problem of an incompressible power-law fluid flowing at zero Reynolds number in a channel with a solid friction law at the boundary. From a practical point of view, the main concern here is that the parts of the bed on which sliding occurs are not known *a priori*, but are determined implicitly by inequality constraints on shear stress and velocity at the bed. By analogy with friction problems in elasticity, we develop a variational formulation which is then used to compute numerical solutions in a more systematic manner than in Truffer *et al.* (2001). Lastly, we consider how variations in subglacial water pressure, ice thickness and ice surface slope affect the discharge of a glacier underlain by a plastic till bed. A relationship between these quantities and ice flux is essential in constructing large-scale models of glaciers, but appears to have been considered previously only for glaciers with so-called hard-bed sliding laws at the boundary (e.g. Fowler & Larson 1978; Fowler 1987*a*).

2. Model

We consider a glacier of constant thickness occupying an inclined straight channel of uniform cross-section and align the y-axis of a Cartesian coordinate system with

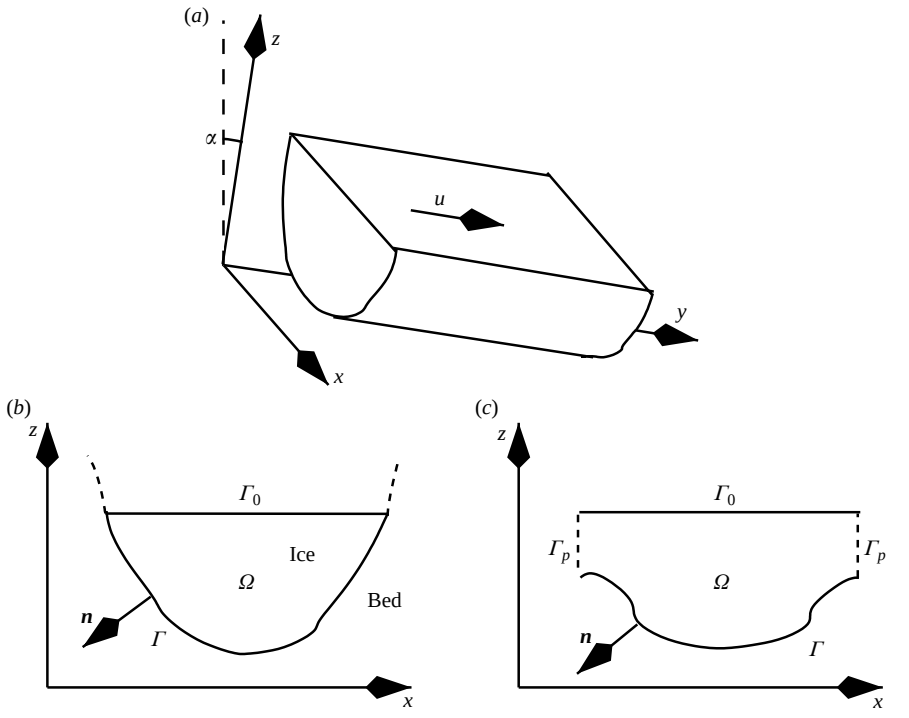

FIGURE 1. The geometry of the problem. The domain shown in (*b*) corresponds to a confined valley glacier, whereas (*c*), where periodic boundary conditions apply along Γ_p, applies to a repeated pattern of ice streams. In this case, the variational method of § 3 still applies, but admissible functions are restricted to the class of functions in $W^{1,p}(\Omega)$ which are periodic on Γ_p in the trace sense.

the downstream direction, while the x-axis is oriented horizontally and at right angles to the downstream direction (see figure 1). We further assume that the mechanical properties of the glacier bed do not depend on y, so the flow of the glacier is uniaxial and oriented in the y-direction (in glaciology, this flow geometry was originally considered for the case of no-slip boundary conditions by Nye 1965). Hence we only need to consider the problem of determining the downstream velocity u in a cross-section Ω of the glacier, which we assume to be a bounded, open and connected subset of the (x, z)-plane with Lipschitz continuous boundary $\partial\Omega$ (so that the divergence theorem and Poincaré's inequality apply). Note that these assumptions imply that there are no longitudinal stresses assoicated with velocity variations in the axial (y-) direction. For a real glacier, the suppression of the y-coordinate can be justified if the cross-sectional shape, thickness and bed properties of the glacier change with y only over distances that are large compared with the thickness of the ice.

Assuming that ice can be modelled as an incompressible power-law fluid with exponent $n > 0$ (Paterson 1994, chap. 5) flowing at zero Reynolds number, the only non-trivial component of the Stokes equations for the velocity field in the ice is

$$-\nabla \cdot \left(a|\nabla u|^{1/n-1}\nabla u\right) = f \qquad \text{on } \Omega, \tag{2.1}$$

where $\nabla = (\partial/\partial x, \partial/\partial z)$, $a > 0$ is a generalized viscosity and $f = \rho g \sin\alpha > 0$ is the downslope component of gravity, with ρ denoting ice density, g acceleration due to gravity and α the angle of inclination of the glacier. Usually, f can be idealized as

a positive constant. Our theory can, however, also accommodate spatial variations in the gravitational body force due to variations in density. The rheological coefficient a, which we assume to be known, can also vary with position as a result of variations in temperature or in water and impurity content of the ice.

We divide the boundary $\partial\Omega$ into two parts, the upper surface Γ_0 which is horizontal and in contact with the atmosphere, and a part Γ which is in contact with the glacier bed. A trivial alteration of the theory also allows us to consider the case of an additional vertical part Γ_p of the boundary along which periodic boundary conditions apply, as indicated by figure 1; this is more relevant to a periodically repeated pattern of ice streams than to a confined valley glacier.

Γ_0 is stress-free, so

$$-a|\nabla u|^{1/n-1}u_n = 0 \qquad \text{on } \Gamma_0, \tag{2.2}$$

where u_n denotes the outward-pointing normal derivative to the boundary. At the bed Γ, we assume that yielding in the till or at the ice–till interface, and hence sliding, will occur when shear stress attains a yield stress τ_c, while there is no sliding below that yield stress. Allowing for now the possibility that ice could slide uphill if basal shear stress were sufficiently negative, we have

$$\left.\begin{aligned} -a|\nabla u|^{1/n-1}u_n &= \tau_c && \text{if } u > 0,\\ -\tau_c \leqslant -a|\nabla u|^{1/n-1}u_n &\leqslant \tau_c && \text{if } u = 0,\\ -a|\nabla u|^{1/n-1}u_n &= -\tau_c && \text{if } u < 0. \end{aligned}\right\} \tag{2.3}$$

Crucially, the parts of Γ on which the three different cases in (2.3) hold are not known *a priori*, but must be found as part of the solution. Naturally, we expect that uphill sliding cannot occur for a positive body force f, and we shall later show that this is indeed true. The last condition in (2.3) then becomes immaterial and we recover the boundary conditions used in Schoof (2004*b*).

In general, the yield stress τ_c will depend on the difference between confining pressure (which is hydrostatic) and porefluid pressure in the underlying till, as well as the local properties of the till, such as grain size distribution. Owing to the absence of deviatoric normal stresses in our flow geometry, τ_c is independent of the velocity field u. In the analysis that follows, we assume consequently that $\tau_c \geqslant 0$ is a known sufficiently smooth function of position along Γ.

3. Weak formulation

Frictional boundary conditions are ubiquitous in elasticity, but appear not to have been used much in fluid mechanical problems. In this section, we use an analogy with the elastic case (e.g. Duvaut & Lions 1976) to re-cast the problem (2.1)–(2.3) in variational form. This allows us to employ abstract methods of convex analysis (Ekeland & Temam 1976) to study various qualitative attributes of the glacier flow problem – such as whether it has solutions at all, which turns out to be the case only under appropriate conditions on basal yield stress τ_c and driving force f. Moreover, our variational approach leads straightforwardly to a numerical algorithm for solving the flow problem based on the minimization of an appropriate functional, which replaces the *ad hoc* method employed by Truffer *et al.* (2001). The theoretical work below is at times somewhat abstract; nevertheless, we hope that some of the subtleties involved will become apparent to those readers unfamiliar with modern variational methods. However, the reader interested only in the glaciological results can fast-forward to §4, where we present our numerical calculations.

Suppose a and u are sufficiently smooth to apply the divergence theorem, and consider any $v \in C^2(\Omega) \cap C^1(\overline{\Omega})$. Multiplying (2.1) by $v-u$ and integrating over Ω yields, on application of the divergence theorem,

$$\int_\Omega f(v-u) = \int_\Omega a|\nabla u|^{1/n-1}\nabla u \cdot \nabla(v-u) - \int_{\partial\Omega} a|\nabla u|^{1/n-1}u_n(v-u). \tag{3.1}$$

Rearranging and using the boundary conditions (2.2) and (2.3) leads to

$$0 = \int_\Omega a|\nabla u|^{1/n-1}\nabla u \cdot \nabla(v-u) - \int_\Omega f(v-u) + \int_{\Gamma_f} \tau_c \mathrm{sgn}\,(u)(v-u) + \int_{\Gamma_r} \left(-a|\nabla u|^{1/n-1}u_n\right)v, \tag{3.2}$$

where Γ_f and Γ_r denote the parts of Γ on which $|u|>0$ and $u=0$, respectively. Noting from (2.3) that $-a|\nabla u|^{1/n-1}u_n v \leqslant \tau_c|v| = \tau_c(|v|-|u|)$ on Γ_r, and that $\tau_c \mathrm{sgn}\,(u)(v-u) \leqslant \tau_c(|v|-|u|)$ because $\tau_c \geqslant 0$, we find that u must satisfy the variational inequality

$$0 \leqslant \int_\Omega a|\nabla u|^{1/n-1}\nabla u \cdot \nabla(v-u) + \int_\Gamma \tau_c(|v|-|u|) - \int_\Omega f(v-u) \tag{3.3}$$

for all admissible v. The practical advantage of considering an inequality of this type rather than the original boundary-value problem (2.1)–(2.3) is that (3.3) no longer contains any explicit reference to the different parts Γ_r and Γ_f of the bed; when solving (3.3) we no longer have to deal directly with the fact that Γ_f and Γ_r are not known from the outset. This is particularly convenient when dealing with the problem numerically.

The variational inequality (3.3) naturally leads to a so-called *weak* formulation of the boundary-value problem (2.1)–(2.3). Following standard procedure (e.g. Evans 1998), we relax our smoothness assumptions on u, and allow functions which do not have the requisite smoothness to satisfy (2.1)–(2.3) pointwise but which satisfy the variational inequality (3.3) to be considered as generalized or weak solutions of the glacier flow problem. The rationale behind this step is twofold. First, any classical solution of the original boundary-value problem is also a solution of the variational inequality (3.3), and by considering weak solutions we therefore also capture the behaviour of classical solutions, provided they do exist. Secondly, considering a wider class of admissible solutions greatly simplifies the analysis of the problem (notably by ensuring that the function spaces used have a suitable topology) while still ensuring that essential physical properties of solutions (such as conservation of energy, see § 3.3) are preserved. We do not, however, address the problem of the regularity (or smoothness) of solutions, and specifically, we do not attempt to derive conditions which ensure that weak solutions also satisfy the original boundary-value problem pointwise. In the same vein, we do not discuss the nature of stress singularities which may occur at the bed; more details on these for the case of constant viscosity ($n=1$) may be found in Schoof (2004*b*).

Let $p = 1 + 1/n$ and let $W^{1,p}(\Omega)$ be the usual Sobolev space endowed with the norm

$$\|v\| = \left(\int_\Omega |v|^p + \int_\Omega |\nabla v|^p\right)^{1/p}. \tag{3.4}$$

We consider any $u \in W^{1,p}(\Omega)$ to be a weak solution of the boundary-value problem (2.1)–(2.3) if it satisfies the variational inequality (3.3) for all $v \in W^{1,p}(\Omega)$. Furthermore, we suppose that $a \in L^\infty(\Omega)$ with $a > a_0 > 0$ almost everywhere in Ω, where a_0 is a constant, while $f \in L^{p^*}(\Omega)$, $f>0$ almost everywhere, and $\tau_c \in L^{p^*}(\Gamma)$, $\tau_c \geqslant 0$ almost everywhere, where $p^* = p/(p-1)$.

Recognizing the (monotone) operator $A : W^{1,p}(\Omega) \mapsto W^{1,p}(\Omega)^*$ defined by

$$\langle Au, v\rangle = \int_\Omega a|\nabla u|^{p-2}\nabla u \cdot \nabla v \tag{3.5}$$

as the Gâteaux derivative of the convex functional $p^{-1}\int_\Omega a|\nabla u|^p$ (Evans 1998, pp. 451–452), standard methods in convex analysis (e.g. Ekeland & Temam 1976, chap. 2) show that (3.3) is equivalent to finding a minimizer $u \in W^{1,p}(\Omega)$ of the functional J defined by

$$J(v) = \frac{1}{p}\int_\Omega a|\nabla v|^p + \int_\Gamma \tau_c|v| - \int_\Omega fv. \tag{3.6}$$

3.1. *Non-existence, existence and uniqueness of solutions*

We anticipate on physical grounds that there cannot be a solution of the original boundary-value problem (2.1)–(2.3) if the total gravitational driving force $\int_\Omega f$ is greater than the maximum friction force $\int_\Gamma \tau_c$ which the bed is able to exert. This is also true of the weak formulation of the problem: if u is a solution, then putting $v = u + C$ in (3.3), where C is a positive constant, shows that the force balance constraint

$$0 \leqslant \int_\Gamma \tau_c|u + C| - \int_\Gamma \tau_c|u| - \int_\Omega fC \leqslant C\left(\int_\Gamma \tau_c - \int_\Omega f\right), \tag{3.7}$$

must be satisfied. Hence we have the solvability condition

$$\int_\Gamma \tau_c - \int_\Omega f \geqslant 0. \tag{3.8}$$

A solvability condition of this type obviously has implications for the applicability of the model; if the bed is too weak, in the sense that (3.8) is not satisfied, then longitudinal stresses, corresponding to variations in u with the downstream coordinate y, must contribute to ensuring force balance, and the model used here must be amended to take account of these stresses.

We now turn to the question of the existence of solutions to (3.3) when (3.8) is satisfied, for which convex analysis (Ekeland & Temam 1976) provides the appropriate tools. The marginal case $\int_\Gamma \tau_c - \int_\Omega f = 0$, in which sliding occurs everywhere on Γ, was treated by Pélissier & Reynaud (1974). The problem then becomes a nonlinear Neumann boundary-value problem with a non-unique solution (more precisely, a solution u exists provided τ_c is sufficiently smooth, and u is unique only up to an additive constant) and, as a consequence, the ice flux carried by the glacier is indeterminate unless we amend the model to take account of stress variations in the suppressed y-direction.

Below, we will be concerned exclusively with the physically more relevant case in which the strong inequality in (3.8) holds. The existence of a solution can then be proved using a number of abstract results, for instance those in Hess (1974), Gastaldi & Tomarelli (1987), or Shi & Shillor (1991) for the case of constant viscosity ($n = 1$). Here we take a more direct approach (most closely allied to that of Hess) and prove that there exists a positive number R_0 such that $J(v) > J(0) = 0$ whenever $\|v\| > R_0$ (roughly speaking, this ensures that $J(\cdot)$ cannot be minimized 'at infinity' in $W^{1,p}(\Omega)$, see also Duvaut & Lions 1976; Kikuchi & Oden 1988). Any u which minimizes $J(\cdot)$ over the closed, convex and bounded set $\{v \in W^{1,p}(\Omega) : \|v\| \leqslant R_0\}$ therefore minimizes $J(\cdot)$ over the whole of $W^{1,p}(\Omega)$ and is a solution of (3.3).

Since $W^{1,p}(\Omega)$ is reflexive and the functional $J(\cdot)$ is convex, proper and lower semi-continuous, such a solution u must exist (Ekeland & Temam 1976, chap. 2).

Take any $v \in W^{1,p}(\Omega)$, define its mean by $\bar{v} = (\text{meas}\,\Omega)^{-1}\int_\Omega v$ and put $\tilde{v} = v - \bar{v}$. This allows us to apply Poincaré's inequality (Evans 1998, p. 275) to $\int_\Omega |\nabla v|^p = \int_\Omega |\nabla \tilde{v}|^p$. Specifically, we find

$$\begin{aligned} J(v) &\geqslant \frac{a_0}{p}\int_\Omega |\nabla v|^p + \int_\Gamma \tau_c |v| - \int_\Omega f v \\ &\geqslant C_1 \|\tilde{v}\|^p + |\bar{v}|\left(\int_\Gamma \tau_c - \int_\Omega f\right) - \int_\Gamma \tau_c |\tilde{v}| - \int_\Omega f\tilde{v} \\ &\geqslant C_1 \|\tilde{v}\|^p + |\bar{v}|\left(\int_\Gamma \tau_c - \int_\Omega f\right) - \left(C_2 \|\tau_c\|_{L^{p^*}(\Gamma)} + \|f\|_{L^{p^*}(\Omega)}\right)\|\tilde{v}\|, \end{aligned} \tag{3.9}$$

where $C_1 > 0$ is a constant which depends only on a_0, p and Ω, while C_2 is the norm of the trace operator from $W^{1,p}(\Omega)$ into $L^p(\Gamma)$.

The last line of (3.9) takes the form

$$J(v) \geqslant \alpha\left[\|\tilde{v}\|\left(\|\tilde{v}\|^{p-1} - \beta\right) + \gamma\,\|\bar{v}\|\right], \tag{3.10}$$

with α, β and γ positive on account of the assumed strict inequality in (3.8). By writing $R = \|\tilde{v}\| + \|\bar{v}\|$ and minimizing the right-hand side of (3.9) over $\|\tilde{v}\|$ while keeping R constant, it is straightforward to show that the right-hand side of (3.10) is positive when

$$\|\tilde{v}\| + \|\bar{v}\| > R_0 = \frac{p-1}{\gamma}\left[\frac{\beta+\gamma}{p}\right]^{p/(p-1)}, \tag{3.11}$$

and is consequently positive when $\|v\| > R_0$. The existence of a solution u with $\|u\| \leqslant R_0$ follows. Notice also that, since $\gamma = (\int_\Gamma \tau_c - \int_\Omega f)/(C_1 \text{meas}(\Omega)^{1/p})$, R_0 tends to infinity and the bound on $\|u\|$ becomes increasingly poor as equality is approached in (3.8).

Proving the uniqueness of weak solutions u is facilitated by first showing that $u \geqslant 0$ almost everywhere. Indeed, inserting $v = \max(u, 0) \in W^{1,p}(\Omega)$ into (3.3) yields

$$-\int_{\Omega^-} a|\nabla u|^p - \int_{\Gamma^-} \tau_c |u| + \int_{\Omega^-} f u \geqslant 0, \tag{3.12}$$

where $\Omega^- = \{(x, y) \in \Omega : u(x, y) < 0\}$ and similarly $\Gamma^- = \{(x, y) \in \Gamma : u(x, y) < 0$ in the trace sense$\}$. Clearly, each term on the left-hand side is non-positive since $a > 0$, $\tau_c \geqslant 0$, $f > 0$ almost everywhere, and moreover the inequality can only hold if $u \geqslant 0$ almost everywhere in Ω.

Suppose then that u_1 and u_2 are distinct solutions. Putting $v = u_2$, $u = u_1$ and vice versa into (3.3) and adding the resulting inequalities yields

$$\int_\Omega a(|\nabla u_1|^{p-2}\nabla u_1 - |\nabla u_2|^{p-2}\nabla u_2)\cdot(\nabla u_1 - \nabla u_2) \leqslant 0. \tag{3.13}$$

However, the left-hand side of (3.13) is strictly positive unless $\nabla(u_1 - u_2) = 0$ almost everywhere (which incidentally confirms the monotonicity of the operator A, and hence the convexity of $J(\cdot)$). From this it follows that $u_1 = u_2 + C$ almost everywhere, where C is a constant which we may assume to be positive without loss of generality. Putting $v = u_2$, $u = u_1$ in (3.3) and using the fact that u_1 and u_2 must both be positive,

we obtain

$$C\left(\int_\Omega f - \int_\Gamma \tau_c\right) = \int_\Gamma \tau_c(|u_2| - |u_1|) - \int_\Omega f(u_2 - u_1) \geqslant 0, \tag{3.14}$$

which contradicts (3.8) with strict inequality unless $C = 0$. Therefore the solution is unique. (We note in passing that uniqueness is assured relatively easily here because the flow direction of the glacier is straightforward to deduce, with $u \geqslant 0$; this is not the case for the more general case of an ice sheet which is not confined to flow down a channel, as discussed in Schoof 2006)

3.2. *Continuous dependence on data*

In this section, we consider the stability of solutions to (3.3) with respect to perturbations in the data functions a, f and τ_c, that is, we seek to establish whether the velocity field u changes continuously (in an appropriate sense) with changes in a, f and τ_c. Perturbations in f and τ_c are of particular practical concern as driving force and yield stress are likely to vary, albeit slowly, along a real glacier channel, and are also likely to evolve in time as a result of changes in subglacial drainage (which affects the yield stress τ_c through changes in porewater pressure in the till) and in glacier surface slope (which changes the downslope component of gravity f as discussed in § 4). It is therefore relevant to ask whether small changes in f and τ_c necessarily correspond to small changes in the velocity field u, or whether they could lead to abrupt changes in flow behaviour.

Suppose that for all $v \in W^{1,p}(\Omega)$, u_1 and u_2 satisfy

$$\int_\Omega a_1|\nabla u_1|^{p-2}\nabla u_1 \cdot \nabla(v - u_1) + \int_\Gamma \tau_1(|v| - |u_1|) - \int_\Omega f_1(v - u_1) \geqslant 0, \tag{3.15}$$

$$\int_\Omega a_2|\nabla u_2|^{p-2}\nabla u_2 \cdot \nabla(v - u_2) + \int_\Gamma \tau_2(|v| - |u_2|) - \int_\Omega f_2(v - u_2) \geqslant 0. \tag{3.16}$$

Assume further that τ_1, τ_2, f_1 and f_2 are such that $\int_\Gamma \tau_i - \int_\Omega f_i$ is bounded below by some fixed $\delta > 0$ for $i = 1, 2$ as $a_1 - a_2$, $\tau_1 - \tau_2$ and $f_1 - f_2$ tend to zero in norm. In that case, our derivation of the bound R_0 for solutions of (3.3) shows that $\|u_1\|$ and $\|u_2\|$ are bounded above uniformly by some R_δ. Putting $v = u_2$ in (3.15), $v = u_1$ in (3.16) and adding, we obtain after some manipulation that

$$\begin{aligned}
&\int_\Omega a_1(|\nabla u_1|^{p-2}\nabla u_1 - |\nabla u_2|^{p-2}\nabla u_2)\cdot(\nabla u_1 - \nabla u_2) \\
&\quad\leqslant \int_\Gamma (\tau_2 - \tau_1)(|u_1| - |u_2|) + \int_\Omega (f_2 - f_1)(u_2 - u_1) \\
&\quad + \int_\Omega (a_2 - a_1)|\nabla u_2|^{p-2}\nabla u_2 \cdot (\nabla u_2 - \nabla u_1) \\
&\quad\leqslant 2C_2 \|\tau_2 - \tau_1\|_{L^{p^*}(\Gamma)} R_\delta \\
&\quad + 2\|f_2 - f_1\|_{L^{p^*}(\Omega)} R_\delta + 2\|a_2 - a_1\|_{L^\infty(\Omega)} R_\delta^p \doteq \Delta,
\end{aligned} \tag{3.17}$$

where C_2 is the norm of the trace operator as before. Using standard stability estimates for the p-Laplacian (e.g. Fernandez Bonder & Rossi 2001), we can manipulate the left-hand side of (3.17) to bound $\|\nabla u_2 - \nabla u_1\|_{L^p(\Omega)}$. As ice is generally taken to be a shear-thinning material with $n \approx 3$, we consider only the case $n \geqslant 1$ and hence $1 < p \leqslant 2$. With p in that range, we have the following inequality, with $C_p \geqslant (p - 1)$

a positive constant which depends only on p:

$$(|\nabla u_1|^{p-2}\nabla u_1 - |\nabla u_2|^{p-2}\nabla u_2)\cdot(\nabla u_1 - \nabla u_2) \geqslant \frac{C_p|\nabla u_1 - \nabla u_2|^2}{(|\nabla u_1| + |\nabla u_2|)^{2-p}}, \tag{3.18}$$

which holds for any two vectors ∇u_1 and ∇u_2. Using Hölder's inequality,

$$\begin{aligned} a_0 \int_\Omega |\nabla u_1 - \nabla u_2|^p &\leqslant \int_\Omega a_1 |\nabla u_1 - \nabla u_2|^p \\ &\leqslant \left(\int_\Omega a_1 \frac{|\nabla u_1 - \nabla u_2|^2}{(|\nabla u_1| + |\nabla u_2|)^{(2-p)}}\right)^{p/2} \left(\int_\Omega a_1 (|\nabla u_1| + |\nabla u_2|)^p\right)^{(2-p)/2}, \end{aligned}$$

and combining this with (3.18) and (3.17),

$$C_p^{p/2} a_0 \|\nabla u_1 - \nabla u_2\|_{L^p(\Omega)}^p \leqslant \left[\|a_1\|_{L^\infty(\Omega)} 2^p R_\delta^p\right]^{(2-p)/2} \Delta^{p/2}, \tag{3.19}$$

where Δ is defined on the last line of (3.17). Hence ∇u is Hölder continuous with respect to perturbations in the data functions.

A stability estimate for u rather than ∇u can also be derived on this basis. Putting $w = u_1 - u_2$ and splitting w into $\bar{w} = (\operatorname{meas}\Omega)^{-1}\int_\Omega w$, $\tilde{w} = w - \bar{w}$ as before, Poincaré's inequality and (3.19) immediately provide a stability estimate for $\tilde{w}$, and it only remains to consider the behaviour of $\bar{w}$ as perturbations in the data functions tend to zero.

Putting $v = u_2$ in (3.15) and using the fact that u_1 and u_2 are positive, we find

$$-\int_\Omega a_1 |\nabla u_1|^{p-2}\nabla u_1 \cdot \nabla \tilde{w} - \int_\Gamma \tau_1 \tilde{w} + \int_\Omega f_1 \tilde{w} \geqslant \bar{w}\left(\int_\Gamma \tau_1 - \int_\Omega f_1\right). \tag{3.20}$$

Using Hölder's inequality,

$$\bar{w} \leqslant \frac{1}{\delta}\left[\|a_1\|_{L^\infty(\Omega)} R_\delta^{p-1} \|\nabla \tilde{w}\|_{L^p(\Omega)} + \left(C_2 \|\tau_1\|_{L^{p^*}(\Gamma)} + \|f_1\|_{L^{p^*}(\Omega)}\right)\|\tilde{w}\|_{L^p(\Omega)}\right]. \tag{3.21}$$

Reversing the roles of u_1 and u_2, we also obtain

$$\bar{w} \geqslant -\frac{1}{\delta}\left[\|a_2\|_{L^\infty(\Omega)} R_\delta^{p-1} \|\nabla \tilde{w}\|_{L^p(\Omega)} + \left(C_2 \|\tau_2\|_{L^{p^*}(\Gamma)} + \|f_2\|_{L^{p^*}(\Omega)}\right)\|\tilde{w}\|_{L^p(\Omega)}\right], \tag{3.22}$$

and combining the last two inequalities, we see that $\bar{w}$ tends to zero at least at the same rate as $\tilde{w}$ when perturbations in the data functions tend to zero.

Consequently, small perturbations in the data functions correspond to small perturbations in the velocity field, provided that the marginal force balance case $\int_\Gamma \tau_c - \int_\Omega f = 0$ is not approached. An obvious drawback of the stability estimates above is that they depend on the parameter δ, which measures how far we are from the marginal force balance case. Specifically, the stability estimates above become increasingly less restrictive when $\delta \to 0^+$, $R_\delta \sim \delta^{-1} \to \infty$. This suggests that, as the marginal case $\int_\Gamma \tau_c - \int_\Omega f = 0$ is approached, solutions could become increasingly badly behaved. In practice, this appears not to be the case, at least for the very regular data functions and domains which we have considered numerically. (It is worth pointing out, however, that the possible 'bad' behaviour of solutions close to the marginal force balance case is not purely related to the non-uniqueness of Pélissier & Reynaud's (1974) solution, as not only $\|\bar{w}\|$ can apparently become large – as would be expected from solutions differing by a constant – but also $\|\tilde{w}\|$).

3.3. *Some qualitative remarks*

(i) Conservation of energy. By putting $v = 0$ and $v = 2u$ in (3.3), we can show that

$$\int_\Omega a|\nabla u|^p + \int_\Gamma \tau_c|u| = \int_\Omega fu \tag{3.23}$$

at a solution u, which expresses the fact that the rate at which work is done on the glacier by gravity (given by the integral on the right-hand side) is equal to the rate at which heat is generated by shearing in the ice and by friction at the bed (the first and second integrals on the left-hand side, respectively).

(ii) Monotonicity of ice flux with respect to gravitational driving force. This result is of importance as it shows that the glacier sliding model studied here does not lead to a multivalued relationship between driving force and ice discharge of the type first employed by Fowler (1987*a*,*b*) to explain glacier surges. To obtain such a relationship, some kind of hydraulic switch which affects τ_c is likely to be necessary, as in Fowler's papers.

Suppose that u_1 and u_2 satisfy (3.15) and (3.16) with $a_1 = a_2 = a$, $\tau_1 = \tau_2 = \tau_c$, and that f_1 and f_2 are constants such that $f_2 > f_1$ and the solvability condition (3.8) is satisfied with strong inequality. From the conservation of energy argument above, we then have

$$\int_\Omega a|\nabla u_1|^p + \int_\Gamma \tau_c|u_1| - \int_\Omega f_1 u_1 = \int a|\nabla u_2|^p + \int_\Gamma \tau_c|u_2| - \int_\Omega f_2 u_2 = 0, \tag{3.24}$$

and it is straightforward to see that we cannot have $u_1 \equiv u_2$ unless $u_1 \equiv u_2 \equiv 0$, a case which we discount as f_1 and f_2 are positive. Define J_1 and J_2 by

$$J_i(v) = \frac{1}{p}\int_\Omega a|\nabla v|^p + \int_\Gamma \tau_c|v| - \int_\Omega f_i v \qquad (i = 1, 2). \tag{3.25}$$

Then, since u_1 uniquely minimizes J_1 and u_2 uniquely minimizes J_2, it follows that $J_1(u_1) < J_1(u_2)$ and $J_2(u_2) < J_2(u_1)$. Adding these inequalities, we find

$$(f_1 - f_2)\int_\Omega (u_1 - u_2) > 0, \tag{3.26}$$

i.e. ice flux $\int_\Omega u$ is a strictly increasing function of body force f, as may be expected intuitively. On physical grounds, we also expect that $\int_\Omega u_2 \geqslant \int_\Omega u_1$ if $\tau_2 \leqslant \tau_1$ and $a_2 \leqslant a_1$ almost everywhere, as these inequalities signify that the bed is weaker and the ice is softer in problem (3.15) than in (3.16). However, monotonicity of flux with respect to changes in yield stress and viscosity is much more difficult to prove mathematically because it does not follow straightforwardly from the variational formulation of the problem.

3.4. *Numerical method*

The simplest way of solving the problem (3.3) numerically is to look for a minimizer of the functional (3.6). Since a solution u must be non-negative almost everywhere, we can restrict the class of admissible functions v to be $K = \{v \in W^{1,p}(\Omega) : v \geqslant 0 \text{ on } \Gamma \text{ in the trace sense}\}$, and the minimization problem (3.6) becomes

$$\min_{v\in K} \tilde{J}(v) : \qquad \tilde{J}(v) = \left[\frac{1}{p}\int_\Omega a|\nabla v|^p + \int_\Gamma \tau_c v - \int_\Omega fv\right], \tag{3.27}$$

which is the variational form of the Signorini-type boundary-value problem considered (with $p = 2$) in Schoof (2004*b*). The use of this constrained minimization problem

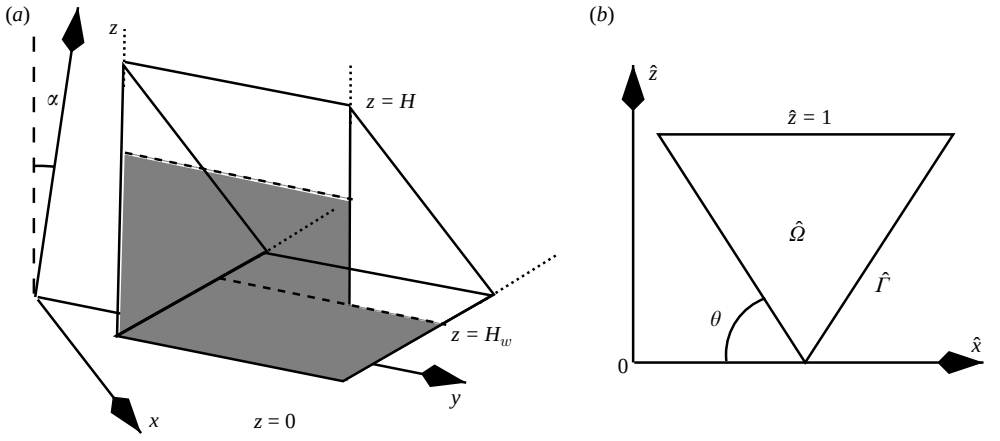

FIGURE 2. (*a*) A three-dimensional view of the problem, with parts of the bed below the water table height shaded in grey. (*b*) The scaled domain $\hat{\Omega}$. θ is the angle between the sloping glacier sides and the horizontal, where $0 < \theta < \pi/2$.

has the advantage of avoiding the non-differentiability of the friction functional $\int_\Gamma \tau_c |v|$, while inequality constraints need only be imposed at the boundary (one could equally have considered the admissible class of non-negative v, but this would be computationally much less efficient). The problem is then discretized using piecewise linear finite elements; a discussion of the convergence of the approximate solution to u for the Newtonian case $p = 2$ may be found in Van Bon (1988). The resulting finite dimensional minimization problem is fairly straightforward to solve using a projected block relaxation method (Glowinski 1984, § 5.3), with individual minimizations being carried using the Polak–Ribière conjugate gradient algorithm. In the general, nonlinear case, a stopping criterion based on (3.23) was used.

4. Results

In this section, we will mostly be interested in the effect of till failure on the discharge $Q = \int_\Omega u$ of a valley glacier, as Q ultimately determines through mass conservation how the profile of the glacier in the downstream (y-) direction changes over time. Implicit here is, of course, that ice thickness and ice flux can change with y, which may appear to be at variance with the assumptions underlying our model. Naturally, we are assuming that variations in ice thickness and ice flux occur over length scales which are large compared with ice thickness and channel width, so that our uniaxial channel flow assumption is justified in the same way as the usual lubrication approximation for glacier flow (Fowler & Larson 1978).

Following Reynaud (1973) and Pélissier & Reynaud (1974), we suppose that the bed has a constant friction coefficient μ and no cohesiveness, so that the yield stress τ_c takes the form

$$\tau_c = \mu(p_i - p_w), \tag{4.1}$$

where p_i is ice overburden pressure and p_w is porewater pressure. We assume further that $z = 0$ and $z = H$ denote the lowest point on the bed and the upper surface of the glacier, respectively (figure 2). Suppose that the water pressure p_w depends linearly on depth below a water table elevation $z = H_w$ in such a way that a hydraulic gradient only exists on the downstream (y-) direction (Reynaud 1973; Pélissier &

Reynaud 1974). Then, taking account of the finite inclination of the glacier (see figure 2) we have $p_w = \rho_w g(H_w - z)\cos\alpha$ for $z < H_w$, $p_w = 0$ for $z \geqslant H_w$, where ρ_w is the density of water. Meanwhile, our uniaxial channel flow assumption reduces the ice overburden pressure to $p_i = \rho g(H - z)\cos\alpha$, and

$$\tau_c = \begin{cases} \mu\rho g \cos\alpha\,(H - z) & (z \geqslant H_w), \\ \mu\cos\alpha\,[\rho g(H - z) - \rho_w g(H_w - z)] & (z < H_w). \end{cases} \tag{4.2}$$

In a real glacier, H_w is likely to be determined by a channelized subglacial drainage system. Assuming that a subglacial channel exists at the lowest point of the bed, the effective pressure in the channel is $N = \rho g H - \rho_w g H_w$, and the simplest subglacial drainage models (e.g. Röthlisberger 1972) calculate N, and hence H_w, as a function of water flux in the channel. We exclude cases in which $\rho_w H_w > \rho H$, $N < 0$ from consideration, as these correspond to water pressure at the lowest point of the bed above ice overburden and therefore to partial flotation of the glacier. While such high water pressures do occur in practice, they are by necessity short-lived as incipient flotation of the ice will usually open up subglacial channels and allow water to drain out. In a pseudo-steady drainage model, in which water pressure is hydrostatic above the base of the glacier, we therefore expect $\rho_w H_w \leqslant \rho H$ (see also Röthlisberger 1972).

Below, we consider only the effects of changing H, H_w and α on the discharge of the glacier, as these reflect changes in glacier geometry and subglacial drainage which occur as a glacier evolves in time. For a real glacier, we ought to distinguish between the angle of inclination of the glacier channel and the glacier surface slope. The former will usually be fixed for a given glacier, while the latter can evolve over time. Our channel flow assumption strictly speaking requires both to be equal, but still provides a good approximation so long as the difference between the two angles is small compared with unity, angles being measured in radians (this is the basis of the usual lubrication approximation for glacier flow, see Fowler & Larson 1978). In that case, α must be identified with the surface slope, which explains why we can consider α to be a variable parameter for a given glacier.

To simplify matters further, we treat the model parameters a, n, μ, ρ and ρ_w as fixed constants. Moreover, we restrict ourselves to triangular glacier cross-sections as indicated in figure 2. Although glacier valleys often have a 'u-shaped' cross-section, approximately triangular cross-sections are sometimes realized in practice, as figure 2 of Lliboutry & Reynaud (1981) shows. Assuming a channel with triangular cross-section here has the advantage of yielding a domain Ω whose shape is independent of ice thickness H (specifically, the scaled domain $\hat{\Omega}$ below is independent of ice thickness H), which in turn reduces the number of independent parameters in the problem and allows our results to be visualized more easily. To exploit this fact, we scale the model by putting

$$\left.\begin{aligned} (\hat{x}, \hat{z}) = \frac{(x, z)}{H}, \quad \hat{u} = \frac{a^n}{(\rho g \sin\alpha)^n H^{n+1}} u, \quad \hat{\tau}_c = \frac{1}{\rho g H \sin\alpha}\tau_c, \\ \hat{Q} = \frac{a^n}{(\rho g \sin\alpha)^n H^{n+3}} Q, \end{aligned}\right\} \tag{4.3}$$

and defining the parameters

$$r = \frac{\rho}{\rho_w}, \qquad \hat{N} = \frac{\rho g H - \rho_w g H_w}{\rho g H} = \frac{N}{\rho g H}, \qquad \hat{f} = \frac{\tan\alpha}{\mu}. \tag{4.4}$$

$\hat{N}$ is a scaled effective pressure at the lowest point of the bed, while $\hat{f}$ a scaled body force. Our requirement that flotation should not take place becomes $\hat{N} \geqslant 0$. $\hat{\tau}_c$ takes the form

$$\hat{\tau}_c = \begin{cases} \hat{f}^{-1}(1-\hat{z}) & (\hat{z} \geqslant r(1-\hat{N})), \\ \hat{f}^{-1}(\hat{N} + (r^{-1}-1)\hat{z}) & (\hat{z} < r(1-\hat{N})). \end{cases} \tag{4.5}$$

Note that we have chosen the scales in (4.3) so that the scaled driving force $\hat{f}$ appears as a coefficient in $\hat{\tau}_c$ rather than as a body force, as equation (4.7) below shows. The rationale behind this is that we are less interested in the effect of the body force $f = \rho g \sin\alpha$ on deformation in the ice than in its effect on sliding. By choosing our scales such that $\hat{f}$ appears as a coefficient in the definition of $\hat{\tau}_c$, we have ensured that the scaled discharge $\hat{Q}$ is constant for a given glacier cross-section when there is no sliding, regardless of the value of $\hat{f}$. Naturally, when the scaled quantities defined above are converted back to their unscaled equivalents, we find that

$$Q \propto f^n H^{n+3} \hat{Q}, \tag{4.6}$$

the constant of proportionality being independent of H, H_w and α. Hence, Q does increase with f as $Q \propto f^n$ even if the scaled flux $\hat{Q}$ remains constant, as is the case when there is no sliding. Removing this dependence on f in the scaled variables ensures that our numerical solutions for different values of $\hat{f}$ are easier to compare when displayed graphically.

Given the non-dimensionalization above, the scaled version of the minimization problem (3.6) is to find a minimizer $\hat{u} \in W^{1,p}(\hat{\Omega})$ of the functional $\hat{J}$ defined by

$$\hat{J}(\hat{v}) = \int_{\hat{\Omega}} |\hat{\nabla}\hat{v}|^p + \int_{\hat{\Gamma}} \hat{\tau}_c |\hat{v}| - \int_{\hat{\Omega}} \hat{v}, \tag{4.7}$$

where $\hat{\nabla} = (\partial/\partial\hat{x}, \partial/\partial\hat{z})$, and $\hat{\Omega}$ and $\hat{\Gamma}$ are the obvious scaled versions of Ω and Γ. Importantly, $\hat{\Omega}$ and $\hat{\Gamma}$ are independent of H and depend only on the angle of inclination θ of the glacier sides (figure 2). The scaled discharge $\hat{Q} = \int_{\hat{\Omega}} \hat{u}$ therefore depends only on the parameters $\hat{f}$, $\hat{N}$, r, p and θ, and on the scaled domain $\hat{\Omega}$. Of these, only $\hat{f}$ and $\hat{N}$ depend on ice thickness H, water-table height H_w and the surface slope α (although this holds true only for triangular cross-sections; for more general channel shapes the scaled domain $\hat{\Omega}$ and boundary $\hat{\Gamma}$ do depend on H). Consequently, for a given cross-sectional geometry defined by θ, we consider discharge $\hat{Q} = \hat{Q}(\hat{f}, \hat{N})$ as a function of scaled effective pressure $\hat{N}$ and body force $\hat{f}$, while we treat r and p as constants, with numerical values $r = 0.9$ (based on $\rho = 900$ kg m^{-3}, $\rho_w = 1000$ kg m^{-3}) and $p = 4/3$ (based on the widely used value $n = 3$ in Glen's law for the rheology of ice, see Paterson 1994, chapter 5).

4.1. *Numerical results*

Figure 3 shows plots of discharge $\hat{Q}$ versus effective pressure $\hat{N}$ at various values of the body force $\hat{f}$ for three different channel shapes, with $\theta = \pi/8$, $\pi/4$ and $\pi/3$. The values used for $\hat{f}$ are motivated by realistic glacier geometries and till friction coefficients. With $\mu = 1$, the values $\hat{f} = 0.08745$, 0.1763 and 0.3640 correspond to surface slopes $\alpha = 5°$, 10° and 20°, respectively. $\mu = 1$ is somewhat large compared with experimentally determined friction coefficients: Iverson *et al.* (1998) give $\mu = 0.5$ for till from a Swedish mountain glacier, in which case the values of $\hat{f}$ above correspond to surface slopes $\alpha = 2.4°$, 5° and 10.3°, respectively. A noteworthy point, however, is that the ring-shear tests typically employed to measure friction coefficients

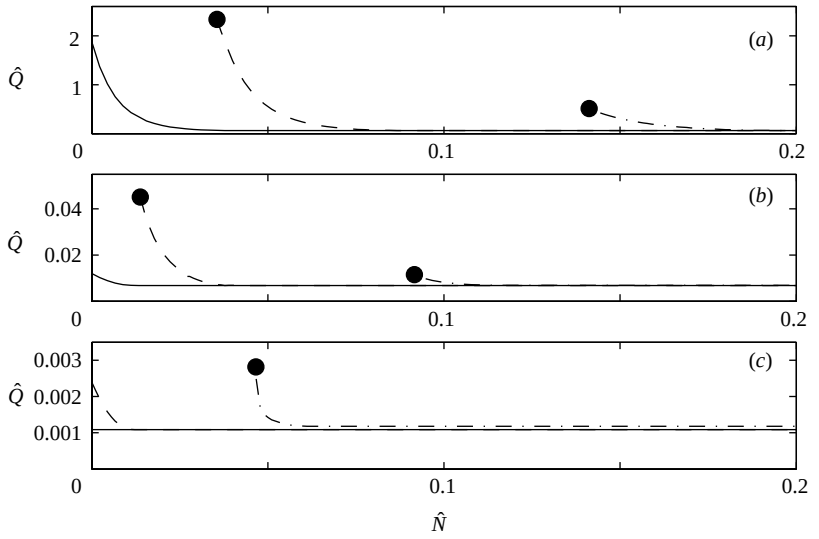

FIGURE 3. Discharge $\hat{Q}$ against effective pressure $\hat{N}$ for channels with (*a*) $\theta = \pi/8$, (*b*) $\theta = \pi/4$ and (*c*) $\theta = \pi/3$. In each plot, the solid line corresponds to $\hat{f} = 0.08745$, the dashed line to $\hat{f} = 0.1763$, and the dot-dashed line to $\hat{f} = 0.3640$. A solid circle signifies the value of $\hat{N} = \hat{N}_c$ corresponding to equality in the force-balance constraint (3.8). At that value of $\hat{N}$, the boundary-value problem (2.1) can be re-cast as a Neumann boundary-value problem with $-a|\nabla u|^{1/n-1}u_n = \tau_c$ on Γ, $u \geqslant 0$ on Γ replacing (2.3). The $\hat{Q}$-coordinate of each solid circle corresponds to the smallest solution u of that boundary-value problem; any larger value of $\hat{Q}$ is also attainable at the same value of $\hat{N}$. For smaller values of $\hat{N}$, (3.8) is violated.

for subglacial sediment require the removal of larger rock fragments prior to testing and may consequently underestimate μ.

The most obvious feature of figure 3 is that, for sufficiently steep and wide glaciers (sufficiently large $\hat{f}$ and small θ), effective pressure $\hat{N}$ cannot be lowered below a critical value $\hat{N}_c$ without violating the force balance constraint (3.8). In fact, a simple calculation reveals that the dimensionless equivalent of (3.8) can be written as

$$\int_{\hat{\Gamma}} \hat{\tau}_c - \int_{\hat{\Omega}} 1 = (1 - r(1-\hat{N})^2)\hat{f}^{-1}\operatorname{cosec}\theta - \cot\theta \geqslant 0, \tag{4.8}$$

and hence that force balance requires

$$\hat{N} \geqslant \hat{N}_c = 1 - \sqrt{r^{-1}(1 - \hat{f}\cos\theta)}. \tag{4.9}$$

Note that $\hat{N}_c$ increases with $\hat{f}$ and decreases with θ as indicated above. The reason for this dependence is obvious: force balance depends on having a maximum friction force larger than or equal to the total driving force, which is more likely to be realized at low effective pressures when the ratio of bed circumference to cross-sectional area is large (i.e. when θ is close to $\pi/2$) and when the glacier surface slope is small (i.e. when $\hat{f}$ is small). If we recall that negative $\hat{N}$ corresponds to incipient flotation of the glacier, which we exclude from consideration, then it is clear that the constraint (4.9) is only relevant if $\hat{N}_c$ is positive. This is the case provided $\hat{f}\cos\theta > 1 - r$. For sufficiently low-angled glaciers, it is therefore possible that no positive $\hat{N}$ leads to force balance violation. Regardless of the channel side inclination θ, this always happens

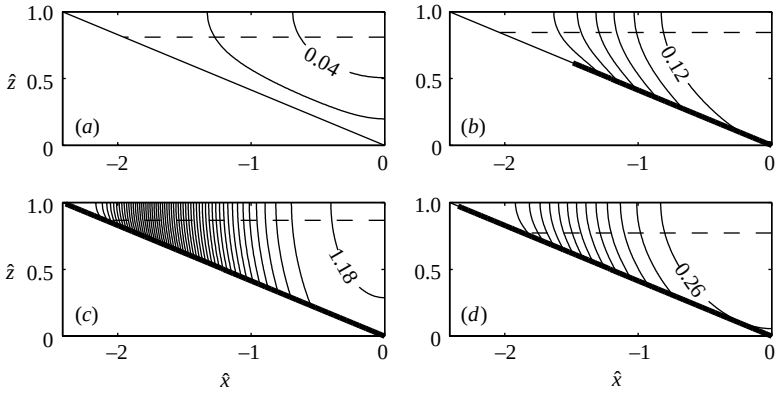

FIGURE 4. Contours of velocity $\hat{u}$ for a channel with $\theta = \pi/8$ (plotted with true aspect ratios; only half the channel is plotted in each case because of the obvious symmetry). Thick lines at the bed indicate regions of sliding, the dashed horizontal line the water-table elevation. Contour interval is 0.02, with contour elevation increasing from left to right; only the highest contour is labelled. (*a*)–(*c*) $\hat{f} = 0.1763$, with effective pressure decreasing: (*a*) $\hat{N} = 0.1$, (*b*) $\hat{N} = 0.06$ and (*c*) $\hat{N} = \hat{N}_c = 0.03558$. (*d*) The critical force balance case for $\hat{f} = 0.3649$, $\hat{N} = \hat{N}_c = 0.1412$. Comparison of (*c*) and (*d*) shows that vertical shearing in the centre of the channel is stronger in (*d*) which explains the lower ice velocities.

when $\hat{f} < 1 - r = 0.1$, which clearly favours the formation of low-angled till-bedded glaciers, for which $\hat{f}$ is small and force balance violation is unlikely to occur.

In cases where $\hat{N}_c$ is positive, our numerical results show that as $\hat{N}$ approaches $\hat{N}_c$ from above, discharge $\hat{Q}$ remains bounded. In fact, figure 3(*a*) suggests that $\hat{Q}$ may even have a bounded derivative with respect to $\hat{N}$ for all $\hat{N} > \hat{N}_c$, though our stability estimates in § 3.2 are too crude to justify either of these statement theoretically.

For $\hat{N}$ larger than the critical value $\hat{N}_c$, we find that the dimensionless flux $\hat{Q}$ is generally an increasing function of the scaled body force $\hat{f}$ and a decreasing function of scaled effective pressure $\hat{N}$. These dependences are, however, not strict. In all cases considered, $\hat{Q}$ is independent of $\hat{N}$ for $\hat{N}$ sufficiently large and $\hat{f}$ sufficiently small. This corresponds to the case in which effective pressures are high enough to prevent sliding below the water table (sliding above the water table as shown in figure 5(*a*) is unaffected by changing $\hat{N}$, so long as there is no sliding below the water table). As $\hat{N}$ is lowered, $\hat{Q}$ then in most cases begins to increase as a result of sliding below the water table elevation. The range of values of $\hat{N}$ for which sliding below the water table happens, and the concomitant increase in $\hat{Q}$, is considerably larger for wider channels than narrower ones, as comparison of figures 3(*a*) and 3(*c*) shows. The more significant increase in discharge caused by sliding in wider glaciers can be understood easily by reference to figure 4; in a wide glacier, the relevant length scale over which shearing in the ice occurs at low values of $\hat{N}$ is the width of the glacier rather than the ice thickness, and this allows higher velocities and hence higher ice discharges to be attained than for narrow glaciers.

The increase in $\hat{Q}$ due to sliding before force balance violation also tends to be larger for smaller $\hat{f}$, for a given glacier cross-section. To understand this, note that $\hat{f}$ appears as a coefficient in the prescription of $\hat{\tau}_c$ in (4.5), where it controls the rate at which yield stress increases as $\hat{z}$ increases between the lowest point of the channel ($\hat{z} = 0$) and the water table elevation ($\hat{z} = r(1 - \hat{N})$). For small $\hat{f}$, that increase in $\hat{\tau}_c$ is larger than for large $\hat{f}$, making the lowest parts of the bed relatively weaker than

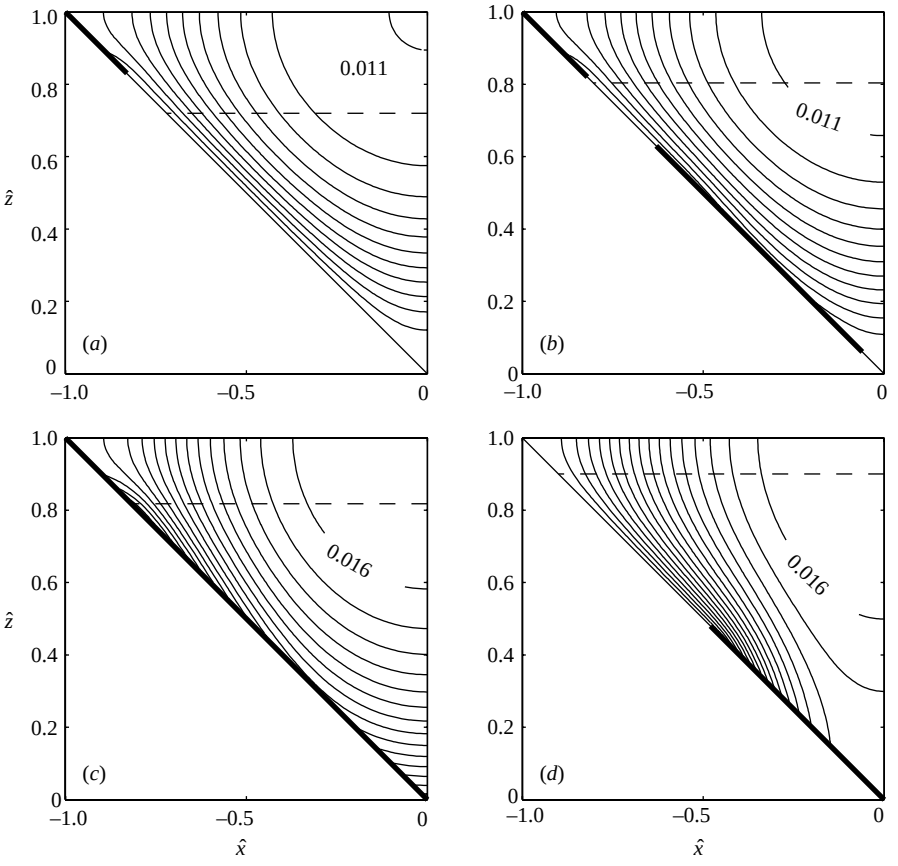

FIGURE 5. As figure 4, but with $\theta = \pi/4$ and a contour interval of 0.001. (*a*)–(*c*) $\hat{f} = 0.364$, with (*a*) $\hat{N} = 0.2$, (*b*) $\hat{N} = 0.107$ and (*c*) $\hat{N} = \hat{N}_c = 0.09164$. (*d*) The case $\hat{f} = 0.08745$ with zero effective pressure $\hat{N} = 0$ at the lowest point of the bed – note the different deformation patterns for high and low $\hat{f}$, with sliding above the water table evident in (*a–c*).

those parts of the bed close to the water table height. As a result, for small $\hat{f}$ and $\hat{N}$ close to its critical value, lateral shearing contributes more to force balance in the central parts of the glacier than vertical shearing compared with the case of larger $\hat{f}$ (compare figures 4(*c*) and 4(*d*)). As a result of this increased lateral shearing, scaled ice velocities $\hat{u}$ in the middle of the glacier and hence scaled discharge $\hat{Q}$ tend to be higher for lower $\hat{f}$ when $\hat{N}$ is close to its critical value. Of course, this only applies to scaled velocities and fluxes (and hence to the structure of the velocity field rather than to absolute velocities): larger dimensional f still corresponds to larger dimensional Q as marginal force balance is approached.

As figures 4, 5 and 6 show, the location of the parts of the bed which are and are not failing is controlled in a non-trivial way by effective pressure, driving stress and channel geometry. For high values of $\hat{f}$ and a sufficiently steep-sided channel geometry, there can be sliding (or till failure) at the highest parts of the bed regardless of effective pressure $\hat{N}$ (e.g. figure 5(*a*)). This results from the fact that effective pressures there are low as a results of the small ice overburden there (with $\hat{\tau}_c = 0$ at the glacier surface) while, at least for narrow channel geometries, relatively

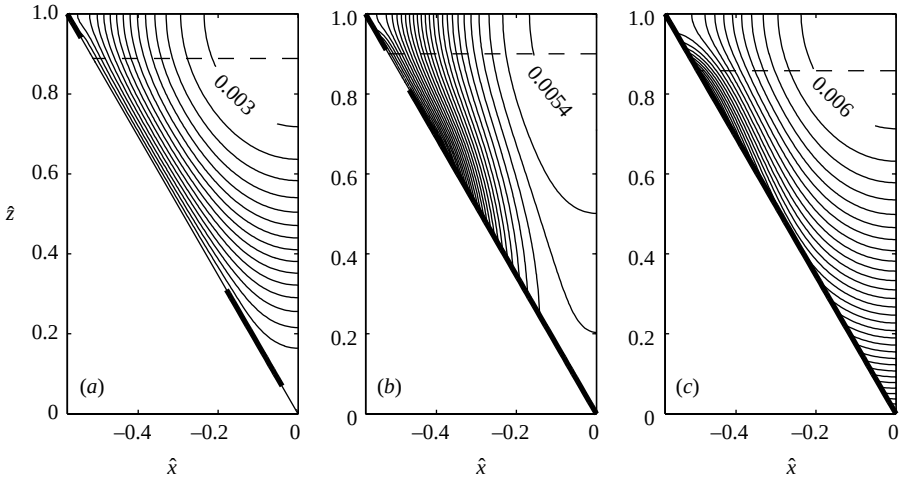

FIGURE 6. As figure 4, but with $\theta = \pi/3$ and a contour interval of 0.0002. (a, b) $\hat{f} = 0.1763$, with (a) $\hat{N} = 0.0125$ and (b) $\hat{N} = 0$, while (c) has $\hat{f} = 0.3640$ and $\hat{N} = \hat{N}_c = 0.04663$. Note that the high $\hat{f}$ case (c) has zero velocity only at the lowest point of the bed, with sliding everywhere else, while the lower $\hat{f}$ case has sliding above and below the water table, with no sliding close to the water table even at zero effective pressure $\hat{N} = 0$.

high shear stress can be realized close to the sides of the glacier. Notably, this till failure occurs in a part of the bed where the till is 'dry', in the sense that it is above the elevation of the water table (which is at $\hat{z} = r(1 - \hat{N})$). As yield stresses above the water table are unaffected by changes in water table elevation, this 'dry' form of sliding is also unaffected by changes in water table elevation, provided the water table remains sufficiently low, corresponding to sufficiently high effective pressures. At lower effective pressures, sliding will generally begin to occur below the water table elevation. For wide channels, this happens first at the lowest point of the bed, with regions of slip spreading up the sides of the channel as effective pressure is lowered (figure 4*b*, *c*). For narrower channel geometries, shear stresses at the lowest point of the bed tend to be somewhat lower than they are higher up the sides of the channel, and a region of till failure tends to form some way up the side of the channel, spreading out from there (figure 5*b* and figure 6*a*). For sufficiently large $\hat{f}$, $\hat{N}$ can then be lowered to its critical value $\hat{N}_c$, at which sliding occurs everywhere at the bed. The location of the last part of the bed which fails as $\hat{N}$ is decreased towards $\hat{N}_c$ also depends on $\hat{f}$ and channel geometry. For wide channels, this is invariably located at the glacier surface (figure 4). For narrower channels, it tends to be closer to the water-table elevation, where bed yield stresses are highest (figure 5*c*). For very narrow channels, the last bed patch to fail can sometimes be located at the lowest point of the bed, because the narrow shape of the domain can make it difficult to generate sufficiently high shear stresses there (figure 6). Whether this is the case or not depends on $\hat{f}$. As described above, the decrease in scaled bed yield strength $\hat{\tau}_c$ between the lowest point of the bed and the water-table elevation is smaller for larger $\hat{f}$, which in turn makes it more likely that the till at the lowest point of the bed will fail last.

5. Discussion

One important limitation on the yield stress model (4.2) in the previous section is its reliance on a hydrostatic decrease in pore water pressure above the lowest point of

the bed. Essentially, we are assuming that the bed is hydrologically 'well-connected', which is often not true in practice, at least over sufficiently short time scales (e.g. Kavanaugh & Clarke 2001). In fact, ice-stream flow represents a scenario diametrically opposed to that considered in § 4. As discussed in Schoof (2004*b*), yield stresses at the bed of ice ridges (the slowly flowing parts of ice sheets which separate rapidly flowing ice streams) must generally be higher than at the bed of ice streams, yet ice ridges do not always correspond to bed topographic highs which could explain a hydrostatic decrease in porewater pressure and hence an increase in yield stress (Raymond *et al.* 2001). A number of factors unrelated to subglacial drainage, such as spatial variations in the mechanical properties of subglacial till, could explain the high sediment yield stresses which must prevail at the base of ice ridges, but a more likely explanation is that water pressures there are simply low, and that a finite hydraulic gradient does exist at the bed between ice ridges and ice streams. A possible explanation for these spatial contrasts in basal water pressure may be thermal and hydraulic feedbacks of the type studied by Fowler & Johnson (1996) and van der Veen & Whillans (1996), which ensure that water pressures are not hydrostatic, at least for a glacier or ice sheet of sufficient horizontal extent. However, given these caveats, our yield stress prescription (4.2) still represents the simplest model for how we might expect basal water pressure to behave in glaciers of relatively limited width, at least when considering time scales large compared with short-term hydraulic events of the type discussed in Kavanaugh & Clarke (2001) and references therein.

As pointed out in § 3.3, the model used here does not independently shed any new light on glacier surge mechanisms. Mathematical surge models (Fowler 1987*b*, 1989; Greenberg & Shyong 1990; Fowler & Schiavi 1998; Schoof 2004*a*) generally require a multi-valued relationship between ice discharge and local glacier geometry, which enters into our problem through f and the ice thickness H. As shown in § 3.3, discharge Q increases monotonically with f. Moreover, our numerical results also show that the scaled discharge $\hat{Q}$ increases as $\hat{N}$ decreases. Assuming for a moment that the dimensional effective pressure $N = \rho g H \hat{N}$ remains constant as glacier thickness H changes (corresponding to constant flux of meltwater in a subglacial channel at the lowest point of the bed, cf. Röthlisberger 1972), we see that $\hat{N}$ decreases as H increases. Hence, from (4.6), it is clear that Q also increases monotonically with ice thickness H, and hence that there is no multivaluedness in the relationship between local glacier geometry and ice discharge. To explain surges within the confines of the mechanical glacier flow model presented here is therefore likely to require an additional description of subglacial drainage in the downstream (y-) direction. This drainage model must then include a switch between different types of drainage systems, and hence between different dimensional effective pressures N, as in Fowler's (1987*b*; 1989) surge theory.

The application of our results to practical glacier dynamics problems faces a further difficulty. Only for relatively low-angled glaciers does the possibility of force balance violation not occur in our model. That is, only for glaciers which have small values of the scaled body force $\hat{f}$ can we lower effective pressure $\hat{N}$ to zero and still compute an ice discharge $\hat{Q}$. For a wide glacier channel ($\theta \ll 1$), we found that $\hat{f} < 1 - r$ is required to render negative the critical value $\hat{N}_c$ below which effective pressure must not drop. Assuming a friction coefficient of $\mu = 1$, this corresponds to an angle of $\alpha < 5.71^\circ$, while $\mu = 0.5$ gives $\alpha < 2.86^\circ$. Although this is a fairly stringent limitation, large glaciers often do have small surface slopes which may fall below this limit (Clarke 1991). Our results could therefore be used as a basis of a highly simplified model for the flow of low-angled till-bedded glaciers, but we must

bear in mind that most glaciers will not have a simple triangular cross-sectional shape.

Many glacier dynamics models (Fowler e.g. 1987*b*; Vieli, Funk & Blatter 2001; Pattyn 2002) rely on the heuristic assumption that sliding velocity u_b at the bed follows a power-law relationship with shear stress at the bed τ_b and local effective pressure p_e, of the form (see Schoof 2005, for a review of hard-bed sliding)

$$u_b = C\tau_b^m p_e^{-n}, \tag{5.1}$$

where C, m and n are positive constants. In their simplest form, models of this type then assume that the contribution Q_s of sliding to ice discharge Q likewise follows a power-law relationship of the same type, roughly of the form $Q_s = CWHu_b = CWH\tau_b^m N^{-n}$, where W is glacier width, H is ice thickness, N is a global measure of effective pressure and $\tau_b = \rho g H \sin\alpha$, where α is the local surface slope (Fowler 1987*a*). In cases where force-balance violation is not an issue – which is the case primarily for low-angled glaciers – our results for Q are qualitatively similar; Q tends to increase when the scaled body force $\hat{f}$ (representing glacier surface slope) and the ice thickness H are increased, and when the scaled effective pressure $\hat{N} = N/(\rho g H)$ is decreased, corresponding to either a decrease in the dimensional effective pressure N or an increase in H. It is worth noting that field measurements corroborate at least some of these results empirically; Jansson (1995) observes that surface velocities on at least one till-bedded glacier increase with decreasing effective pressure, and is able to fit a power-law relationship to these two quantites for a limited range of effective pressures.

These results lead us to conclude that models assuming power-law relationships between discharge, ice thickness, surface slope and effective pressure of the form above may yield results which reflect the qualitative behaviour of some low-angled glaciers with deformable beds. The physical basis for the behaviour of ice discharge Q is, however, different from that assumed by sliding laws of the form (5.1). In the case of simple models using (5.1), sliding velocity is assumed to be an increasing function of local shear stress and a decreasing function of effective pressure, usually as a result of processes involved in sliding over undeformable beds (e.g. Fowler 1987*a*). In our solid friction model, sliding velocity is not determined by local shear stress and effective pressure at the bed (indeed, effective pressure determines shear stress independently of sliding velocity, so long as there is sliding). Instead, the dependence of Q on the effective pressure $\hat{N}$ and driving force $\hat{f}$ arises because the extent of bed patches on which sliding occurs increases with $\hat{f}$ and decreases with $\hat{N}$.

As mentioned above, the applicability of our two-dimensional model and the similarities between it and more classical prescriptions for ice discharge Q are limited to relatively low-angled glaciers, or cases in which effective pressure is sufficiently large. The spectre of force balance violation in our model does not imply that real glaciers are likely to start accelerating in the Newtonian sense as large ice avalanches; it merely points to the fact that our channel flow model, in which longitudinal stresses arising from variations in u with respect to the downstream coordinate y are ignored, has limited applicability. In practice, longitudinal stresses are likely to ensure force balance when the maximum friction force on a glacier cross-section is locally less than the total driving force acting on that cross-section. It is therefore natural to look for simplified models which can account for longitudinal as well as lateral shear stresses. Short of solving the full Stokes equations for a three-dimensional glacier, the most promising approach is to consider depth-integrated models which arise at leading order in asymptotic expansions of the Stokes equations for ice masses with low aspect

ratios. Suffice it to point out here that the 'shelfy stream' equations considered by e.g. MacAyeal, Bindschadler & Scambos (1995), but with Coulomb-type friction rather than a 'hard-bed' sliding law, are susceptible to a variational treatment analogous to that used here. Similar solvability conditions to (3.8), now ensuring moment as well as force balance, arise in that treatment, with Korn's second inequality (Wang 2003) replacing Poincaré's inequality in their derivation; details of this theory are reported in Schoof (2006).

6. Conclusions

This paper has set out a consistent theoretical treatment of glacier flow over a Coulomb-plastic bed. Its practical use is mostly in providing a numerical method for solving the problem, and in proving various qualitative attributes of solutions such as the solvability condition (3.8), the positivity of the velocity field u and the monotonicity of ice discharge $Q = \int_\Omega u$ with respect to driving force f. Although we focused our attention on valley glaciers in this paper, the numerical method employed here can also be used to study the shear margins of ice streams overlying plastic till.

The second half of the paper focused on the relationship between discharge in a valley glacier and ice thickness, surface slope and subglacial effective pressure. The most important result here is that effective pressure at the lowest point of the bed must generally remain above a critical value in order to ensure local force balance; when effective pressure drops below that value, longitudinal stresses in the ice must become important. The (dimensional) critical value of effective pressure which controls this switch in behaviour depends on the surface slope and thickness of the glacier, and decreases with increasing ice thickness and surface slope. For sufficiently low-angled glaciers, this critical value is negative and effective pressure at the lowest point of the bed – where we envisage a subglacial drainage channel to exist – can be lowered to zero without causing a local force balance violation.

When local force balance violation is not an issue, the discharge of a glacier generally increases with ice thickness and surface slope, and decreases with effective pressure. These dependences are also a feature of classical glacier dynamics models, which often assume that sliding velocity at the bed is an increasing function of basal shear stress and a decreasing function of effective pressure. The physical basis for this behaviour is different in the present case, as increased discharge results from the formation of larger bed patches on which sliding occurs rather than from a local dependence of sliding velocity on bed shear stress and effective pressure. Nevertheless, this result indicates that the results of classical glacier dynamics models may also qualitatively apply to some till-bedded glaciers.

I would like to thank Emanuele Schiavi and Ian Frigaard for their advice on various technical matters, and the anonymous referees as well as the associate editor, Grae Worster, for their thorough scrutinity of this paper. This work was supported by a Killam postdoctoral research fellowship at the University of British Columbia.

REFERENCES

Adams, M. J., Aydin, I., Briscoe, B. J. & Sinha, S. K. 1997 A finite element analysis of the squeeze flow of an elasto-viscoplastic paste material. *J. Non-Newtonian Fluid Mech.* **71**, 41–57.

Alley, R. B. & Bindschadler, R. A. (ed.) 2001 *The West Antarctic Ice Sheet: Behaviour and Environment*. American Geophysical Union, Washington, DC.

Clarke, G. K. C. 1991 Length, width and slope influences on glacier surging. *J. Glaciol.* **37**, 236–246.

Duvaut, G. & Lions, J. L. 1976 *Inequalities in Mechanics and Physics*. Springer.

Ekeland, I. & Temam, R. 1976 *Convex Analysis and Variational Problems*. North-Holland.

Evans, L. C. 1998 *Partial Differential Equations*. American Mathematical Society, Providenc.

Fernandez Bonder, J. & Rossi, J. D. 2001 Existence results for the p-Laplacian with nonlinear boundary conditions. *J. Math. Anal. Appl.* **263**, 195–223.

Fowler, A. C. 1981 A theoretical treatment of the sliding of glaciers in the absence of cavitation. *Phil. Trans. R. Soc. Lond.* **298** (1445), 637–685.

Fowler, A. C. 1987*a* Sliding with cavity formation. *J. Glaciol.* **33**, 255–267.

Fowler, A. C. 1987*b* A theory of glacier surges. *J. Geophys. Res.* **92** (B9), 9111–9120.

Fowler, A. C. 1989 A mathematical analysis of glacier surges. *SIAM J. Appl. Maths* **49**, 246–263.

Fowler, A. C. 2003 On the rheology of till. *Ann. Glaciol.* **37**, 55–59.

Fowler, A. C. & Johnson, C. 1996 Ice-sheet surging and ice-stream formation. *Ann. Glaciol.* **23**, 68–73.

Fowler, A. C. & Larson, D. A. 1978 On the flow of polythermal glaciers. I. Model and preliminary analysis. *Proc. R. Soc. Lond* A **363**, 217–242.

Fowler, A. C. & Schiavi, E. 1998 A theory of ice-sheet surges. *J. Glaciol.* **44**, 104–118.

Gastaldi, F. & Tomarelli, F. 1987 Some remarks on nonlinear and noncoercive variational inequalities. *Boll. Un. Mat. Ital.* **1-B** (7), 143–165.

Glowinski, R. 1984 *Numerical Methods for Nonlinear Variational Problems*. Springer.

Greenberg, J. M. & Shyong, W. 1990 Surging glacial flows. *IMA J. Appl. Maths* **45**, 195–223.

Harrison, W. D., Echelmeyer, K. A. & Larson, C. F. 1998 Measurement of temperature in a margin of Ice Stream B, Antarctica: implications for margin migration and lateral drag. *J. Glaciol.* **44**, 615–624.

Hess, P. 1974 On semi-coercive nonlinear problems. *Indiana U. Maths J.* **23**, 645–654.

dell'Isola, F. & Hutter, K. 1998 What are the dominant thermomechanical processes in the basal sediment layer of large ice sheets? *Proc. R. Soc. Lond.* A **454**, 1169–1195.

Iverson, N. R., Baker, R. W., Hooke, R. LeB., Hanson, B. & Jansson, P. 1999 Coupling between a glacier and a soft bed: I. A relation between effective pressure and local shear stress determined from till elasticity. *J. Glaciol.* **45**, 31–40.

Iverson, N. R., Hooyer, T. S. & Baker, R. W. 1998 Ring-shear studies of till deformation: Coulomb-plastic behaviour and distributed shear in glacier beds. *J. Glaciol.* **44**, 634–642.

Jansson, P. 1995 Water pressure and basal sliding on Storglaciären, northern Sweden. *J. Glaciol.* **41**, 232–240.

Kamb, B., Raymond, C. F., Harrison, W. D., Engelhardt, H., Echelmeyer, K. A., Humphrey, N., Brugman, M. M. & Pfeffer, T. 1985 Glacier surge mechanism: 1982–1983 surge of Variegated Glacier, Alaska. *Science* **227**, 469–479.

Kavanaugh, J. L. & Clarke, G. K. C. 2001 Abrupt glacier motion and reorganization of basal shear stress following the establishment of a connected drainage system. *J. Glaciol.* **47**, 472–480.

Kikuchi, N. & Oden, J. T. 1988 *Contact Problems in Elasticity : a Study of Variational Inequalities and Finite Element Methods*. Philadelphia: SIAM.

Lliboutry, L. & Reynaud, L. 1981 'Global dynamics' of a temperate valley glacier, Mer de Glace, and past velocities deduced from Forbes' bands. *J. Glaciol.* **27**, 207–226.

MacAyeal, D. R., Bindschadler, R. A. & Scambos, T. A. 1995 Basal friction of Ice Stream E, West Antarctica. *J. Glaciol.* **41**, 247–262.

Nye, J. F. 1965 The flow of a glacier in a channel of rectangular, elliptic or parabolic cross-section. *J. Glaciol.* **5**, 661–690.

Paterson, W. S. B. 1994 *The Physics of Glaciers*, 3rd edn. Pergamon.

Pattyn, F. 2002 Transient glacier response with a higher-order numerical ice-flow model. *J. Glaciol.* **48**, 467–477.

Pélissier, M. C. & Reynaud, L. 1974 Étude d'un modèle d'écoulement de glacier. *C. R. Acad. Sci. Paris* **279**, 531–534.

Raymond, C. F., Echelmeyer, K. A., Whillans, I. M. & Doake, C. S. M. 2001 Ice stream shear margins. In *The West Antarctic Ice Sheet: Behaviour and Environment* (ed. R. Alley & R. Binschadler), pp. 137–155. American Geophysical Union, Washington, DC.

Reynaud, L. 1973 Flow of a valley glacier with a solid friction law. *J. Glaciol.* **12**, 251–258.

Röthlisberger, H. 1972 Water pressure in intra- and subglacial channels. *J. Glaciol.* **11**, 177–203.

Schoof, C. 2004*a* Bed topography and surges in ice streams. *Geophys. Res. Letts.* **31**, L06401, doi:10.1029/2003GL018807.

Schoof, C. 2004*b* On the mechanics of ice stream shear margins. *J. Glaciol.* **50**, 208–218.

Schoof, C. 2005 The effect of cavitation on glacier sliding. *Proc. R. Soc. Lond.* A **461** 609–627, doi:10.1098/rspa.2004.1350.

Schoof, C. 2006 A variational approach to ice-stream flow. *J. Fluid Mech.* (in press).

Sherwood, J. D. & Durban, D. 1998 Squeeze flow of a Herschel–Bulkley fluid. *J. Non-Newtonian Fluid Mech.* **77**, 115–121.

Shi, P. & Shillor, M. 1991 Noncoercive variational inequalities with application to friction problems. *Proc. R. Soc. Edin.* A **117**, 275–293.

Truffer, M., Echelmeyer, K. A. & Harrison, W. D. 2001 Implications of till deformation on glacier dynamics. *J. Glaciol.* **47**, 123–134.

Tulaczyk, S. 1999 Ice sliding over weak, fine-grained till: dependence of ice-till interactions on till granulometry. *Spec. Paper Geol. Soc. Am.* **337**, 159–177.

Tulaczyk, S., Kamb, W. B. & Engelhardt, H. F. 2000 Basal mechanisms of ice stream b, west antarctica: 1. till mechanics. *J. Geophys. Res.* **105** (B1), 463–481.

Van Bon, T. 1988 Finite element analysis of primal and dual variational formulations of semi-coercive elliptic problems with nonhomogeneous obstacles on the boundary. *Appl. Maths* **33**, 1–21.

van der Veen, C. J. & Whillans, I. M. 1996 Model experiments on the evolution and stability of ice streams. *Ann. Glaciol.* **23**, 129–137.

Vieli, A., Funk, M. & Blatter, H. 2001 Flow dynamics of tidewater glaciers: numerical modelling approach. *J. Glaciol.* **47**, 595–606.

Wang, L. H. 2003 On Korn's inequality. *J. Comput. Math.* **21**, 321–324.